Powder Technology 394 (2021) 1026–1038

Contents lists available at ScienceDirect

Powder Technology

journal homepage: www.elsevier.com/locate/powtec

Development and characterization of magnetic iron oxide nanoparticles using microwave for the combustion reaction ignition, as possible candidates for biomedical applications

Aylin Căpraru [a], Elena-Alina Moacă [a,b,c,*], Cornelia Păcurariu [a,**], Robert Ianoş [a], Radu Lazău [a], Lucian Barbu-Tudoran [d,e]

[a] Politehnica University Timisoara, Faculty of Industrial Chemistry and Environmental Engineering, 6th Pîrvan Blv., Timisoara RO-300223, Romania
[b] "Victor Babes" University of Medicine and Pharmacy Timisoara, Faculty of Pharmacy, 2nd Eftimie Murgu Square, Timisoara RO-300041, Romania
[c] Research Centre for Pharmaco-Toxicological Evaluation, "Victor Babeş" University of Medicine and Pharmacy, 2nd Eftimie Murgu Square, 300041 Timişoara, Romania
[d] Electron Microscopy Laboratory "Prof. C. Craciun", Faculty of Biology & Geology, "Babes-Bolyai" University, 5-7 Clinicilor Street, RO-400006 Cluj-Napoca, Romania
[e] Electron Microscopy Integrated Laboratory, National Institute for R&D of Isotopic and Molecular Technologies, 67-103 Donat Street, RO-400293 Cluj-Napoca, Romania

ARTICLE INFO

Article history:
Received 22 May 2021
Received in revised form 26 August 2021
Accepted 28 August 2021
Available online 15 September 2021

Keywords:
Magnetic iron oxides
Combustion synthesis
Microwave ignition
Stable colloidal suspensions

ABSTRACT

Magnetic iron oxide nanoparticles were prepared by solution combustion synthesis, using iron nitrate as oxidizer and citric acid as fuel. The influence of the combustion reaction ignition procedure, conventional heating and microwave heating, on nanoparticles characteristics was investigated. The synthesized nanoparticles were characterized by scanning and transmission electron microscopy, X-ray powder diffraction, thermogravimetric and differential scanning calorimetry, magnetic measurements, specific surface area and adsorption-desorption isotherms. The magnetic nanoparticles prepared by microwave heating exhibit larger specific surface area (70.7 m^2/g), lower particle medium size (10.7 ± 3.09 nm) and lower saturation magnetization (41.8 emu/g) as compared to the sample prepared by conventional heating. Magnetic nanoparticles prepared by microwave heating were coated with oleic acid and Tween 80, and dispersed in phosphate buffered saline and distilled water. The colloidal suspensions demonstrated good stability, small polydispersity and small values of the hydrodynamic diameter, characteristics which recommend them to be tested for biomedical applications.

1. Introduction

Magnetic nanoparticles are an important class of materials with applications in various fields including catalysis/photocatalysis, ferrofluids, biomedicine, adsorbents in water treatment, magnetic sealing, etc. [1–9]. By far, their biomedical applications are the most interesting being extensively studied by scientists. Magnetic nanoparticles and especially the iron oxides magnetic nanoparticles such as magnetite (Fe_3O_4) and maghemite (γ-Fe_2O_3) have a range of excellent properties which offer them a powerful potential in cancer treatment, carriers for targeted drug delivery, magnetic separation and cellular selection, magnetic resonance imagery (MRI), magnetofection, tissue repair, etc. [10–18]. For biomedical applications, magnetic nanoparticles must combine several properties such as chemical stability, particle size smaller than 100 nm, superparamagnetic behavior at room temperature, high magnetic saturation and a narrow particle size distribution. Moreover, the magnetic nanoparticles need to be coated with a protective layer which must be non-toxic and biocompatible. The biocompatible coating of the surface has to avoid aggregation, sedimentation and biodegradation of magnetic nanoparticles, to ensure high colloidal stability in aqueous carrier as well as to provide appropriate surface properties [19–21]. The employed synthesis method plays an essential role in obtaining magnetic nanoparticles with suitable properties to their further use. At the same time, the synthesis method must be simple, economically advantageous and environmentally friendly. To date, many synthesis routes were developed to produce magnetic iron oxides with tailored properties: co-precipitation [22–25], hydrothermal/solvothermal method [26–28], microemulsion method [19,22,29,30], sonochemical method [22,24,31,32], thermal decomposition [22,33,34], electrochemical method [5,22], etc.. Each of the presented synthesis procedures show different drawbacks for the magnetic iron oxides

* Corresponding author at: "Victor Babes" University of Medicine and Pharmacy Timisoara, Faculty of Pharmacy, 2nd Eftimie Murgu Square, Timisoara RO-300041, Romania.
** Corresponding author at: Politehnica University Timisoara, Faculty of Industrial Chemistry and Environmental Engineering, 6th Pîrvan Blv., Timisoara RO-300223, Romania.
E-mail addresses: alina.moaca@umft.ro (E.-A. Moacă), cornelia.pacurariu@upt.ro (C. Păcurariu).

https://doi.org/10.1016/j.powtec.2021.08.093

preparation [22,32,34]. Even if the precipitation method is by far the most simple and used, because of the mutual influence of the working parameters such as: pH, ionic strength of the solution, temperature, nature of the salts used, concentration of the precipitating agent or the protective atmosphere, by using this method the size distribution of the obtained particles is broad and their shape and size are hardly controlled [22–25]. The main disadvantages of the hydrothermal/solvothermal method are the harsh reaction conditions (high pressure from 0.3 to 4 MPa and long reaction time ranging from several hours to days), the high cost of the work equipment and the impossibility of monitoring the synthesis process [22,24]. The microemulsion method is complicated, requires large amounts of solvent and several washing processes of the surfactant excess. Also, the crystallinity of the particles obtained by this method is low as the reaction temperature is low, ranging between 20 and 80 °C [13,22,24]. The sonochemical method has the disadvantages that is not energy efficient and the shape control of the particles is bad. [22,24,31,32]. Besides the fact that the thermal decomposition of various organometallic precursors method is quite complicated and the reaction time is long, its main disadvantage is the use of toxic solvents and surfactants which may negatively affect the biocompatibility of the product [22,33,34]. The electrochemical method is quite complicated, needs specialized equipment and long reaction time, involving hours or even days for obtaining the magnetic particles [5,22,35,36].

Therefore, developing new simple, flexible and inexpensive methods to synthesize magnetic nanoparticles with tailored properties to provide them the whole potential in biomedical applications is of extreme importance.

Solution combustion synthesis (SCS) is a very promising alternative, which offers several advantages over the methods listed above. Based on the exothermic reaction between an oxidizing agent (the desired metal nitrate) and various reducing agents (fuels), this method is simple, energy saving, fast, versatile, eco-friendly and involves low-cost raw materials. This technique has been used for the synthesis of a wide variety of metal oxides including $ZnAl_2O_4$ [37], $SrAl_2O_4$ [38], $CaMgSi_2O_6$ [39], $Li_2CuP_2O_7$ [40], $2CaO \cdot SiO_2$ [41]. In the latest years, solution combustion synthesis became increasingly used for the preparation of different magnetic nanomaterials such as Fe_3O_4 [42], $MgFe_2O_4$ [43], MFe_2O_4, (M = Co and Ni) [44], Fe_3O_4/Ag/C [45], $CoCrFeO_4$ [46]. The interest for this method is fully justified because its highest advantage is the possibility of obtaining materials with tailored properties by changing the synthesis conditions in large limits. Beside the conventional ignition, in the recent years a special attention has been paid to the microwave ignition of combustion reactions. In the conventional ignition of combustion reactions, there is a temperature gradient between the heat source and the reaction mixture which leads to an inhomogeneous temperature distribution and consequently to a lower temperature of reactants than the set one. In the microwave ignition, the heat is generated in the entire reaction volume which leads to a homogeneous temperature distribution [47–49]. The microwave-assisted solution combustion synthesis was used for the preparation of different materials including ZnO [50], $CdFe_2O_4$ [51], Mg-doped $ZnFe_2O_4$ [52], Fe_3O_4 [53], Zn-doped $NiFe_2O_4$ [54].

According to the literature reports [47,49,53,55,56], some physicochemical properties of materials prepared by microwave ignition are different in comparison to those obtained by using conventional ignition of combustion reactions.

In order to ensure a tailored property of the magnetic nanoparticles surface, different biocompatible surfactants (saturated and unsaturated fatty acids, dextran, polyethylene glycol, Tween 80, starch, chitosan etc.) are used. By far, oleic acid (OA) is the most frequently used surfactant because it forms a dense protective layer providing uniform and monodisperse nanoparticles [57].

The goal of this work is the preparation of magnetic iron oxides that have the characteristics required in biomedical applications by using the solution combustion method. We have used this method because unlike some of the methods presented above it is fast, energy-efficient and environmentally friendly since the reaction by-products are N_2, H_2O and CO_2. In addition, some characteristics of the nanopowders such as the specific surface area and the particle size can be adjusted by simply changing the synthesis conditions.

For this purpose we performed a comparative analysis of the iron oxide nanoparticles characteristics induced by the ignition of the combustion reactions using microwave and conventional heating respectively. In order to assess the potential use of these magnetic nanoparticles for biomedical applications, the effects of a fatty acid (oleic acid) and a nonionic (Tween 80) surfactants, as well as of the dispersion medium (phosphate buffered saline - PBS and distilled water) on the stability and the morphology of the as-prepared colloidal suspensions have been systematically investigated.

2. Materials and methods

2.1. Materials

Ferric nitrate nonahydrate ($Fe(NO_3)_3 \cdot 9H_2O$, citric acid ($C_6H_8O_7$)), vegetal oleic acid 65%–88% (OA - $C_{18}H_{34}O_2$) and Tween 80 (T - $C_{64}H_{124}O_{26}$) were purchased from Merck (Darmstadt, Germany) and phosphate buffered saline (PBS) was achieved from Sigma Aldrich (Darmstadt, Germany). The distilled water was obtained in Faculty of Industrial Chemistry and Environmental Engineering, Timisoara, Romania, using a GFL-2008 distillatory (Gesellschaft für Labortechnik mbH D-30938, Burgwedel, Germany).

2.2. Experimental methodology

2.2.1. Preparation of magnetic iron oxide nanoparticles

Two samples of iron oxide (0.07 mol each) were prepared from ferric nitrate nonahydrate, $Fe(NO_3)_3 \cdot 9H_2O$ and citric acid, $C_6H_8O_7$ mixed in a molar ratio of 6:5. Ferric nitrate nonahydrate (56.5600 g) and citric acid (22.4140 g) were dissolved in 20 mL of distilled water under magnetic stirring (200 rpm). In order to investigate the influence of the combustion reaction ignition procedure on the nanoparticles characteristics, the round bottom flasks containing the clear solution of the ferric nitrate and citric acid were placed inside a heating mantle (450 °C) (namely sample M1 – Fig. 1-A) and in a microwave oven (2.45 GHz, 800 W) (namely sample M2 – Fig. 1-B) respectively. As the solutions were heated up, combustion reaction took place, accompanied by the release of large amounts of gases regardless the ignition procedure. After the combustion reaction was completed, the flask with the tap in the closed position was allowed to cool down to ambient

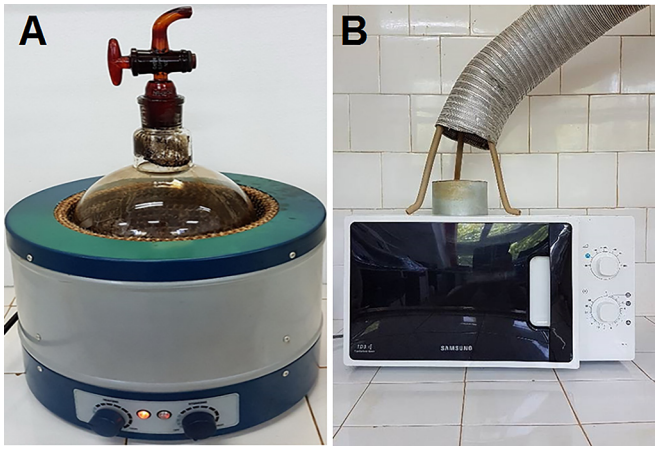

Fig. 1. Ignition of the combustion reaction: heating mantle (A), microwave oven (B).

Table 1
Synthesis conditions and characteristics of the iron oxide powder.

Sample	Ignition procedure	Phase composition	D_{XRD} (nm)	S_{BET} (m^2/g)	Desorption cumulative surface area of pores (m^2/g)	Desorption average pore diameter (nm)	Desorption cumulative volume pores (cm^3/g)
M1	heating mantle	3% γ-Fe_2O_3 + 97% Fe_3O_4	23	41.53	44.38	7.06	0.078
M2	microwave oven	85% γ-Fe_2O_3 + 11% Fe_3O_4 + 2%FeO + 2% Fe	5	70.71	57.11	5.15	0.073

temperature. Distilled water was added to the powders thus obtained, which were afterwards transferred to porcelain dishes and hand ground.

Subsequently, the samples were sonicated for 10 min at 100% amplitude, using a QSonica 700 W device (Newtown, CT, USA). After sonication, the samples were washed with warm distilled water (60–70 °C) on the filter paper, dried in the oven at 70 °C, hand ground and characterized.

2.2.2. Preparation of colloidal suspensions

Since the physicochemical characteristics of the M2 nanoparticles proved to be more suitable for biomedical applications (Table 1), as shown below, these nanoparticles were further used for the preparation of colloidal suspensions. In order to obtain stable colloidal suspensions, two surfactants and two carrier media were employed. The M2 magnetic nanoparticles were coated with oleic acid (OA) and Tween 80 (T) respectively, and dispersed in phosphate buffered saline (PBS) and distilled water as well, according to the schematic protocol depicted in Fig. 2. Stable colloidal suspensions of M2 nanoparticles double coated with oleic acid were prepared by using the slightly modified version of preparation technique previously published by our group [58].

Briefly, in order to coat the M2 magnetic nanoparticles with the first layer of OA, these were moistened in ethanol (96%, *v*/v) aqueous solution for 1 day. The suspension was sonicated for 2 h at 50% amplitude, with 10 s pulse/on and 5 s pulse/off, in order to de-agglomerate the magnetic nanoparticles, making them suitable for the adsorption process. OA was added dropwise to the suspension under vigorous stirring (500 rpm) at 80–82 °C. The M2 magnetic nanoparticles coated with OA monolayer, named OA-M2, were three times washed with warm distilled water (60–70 °C) until the soluble impurities and free oleic acid were removed. The as formed OA-M2 magnetic nanoparticles were further used for the coating with the second layer using OA and Tween 80 respectively, as surfactants.

The single coated OA-M2 magnetic nanoparticles were re-dispersed in distilled water and in PBS respectively, and after adjusting the pH value (pH = 10), the physisorption of the OA second layer took place at 80–82 °C, under vigorous stirring. The magnetic nanoparticles double coated with OA were collected after magnetic decantation and dispersed in 100 mL distilled water and in PBS respectively, by intense sonication at 50% amplitude for 1 h. The as resulted colloidal suspensions are further named SM2-O/W and SM2-O/PBS (Fig. 2).

Stable colloidal suspensions of M2 magnetic nanoparticles coated with Tween 80, were obtained according to the slightly modified method of Wang et al. [59]. The single coated OA-M2 magnetic nanoparticles were re-dispersed in distilled water and in PBS respectively, and a specific amount of Tween 80 was dropwise added into the suspension under vigorous stirring (500 rpm) at 80–82 °C. After magnetic decantation, the magnetic nanoparticles coated with Tween 80 were collected and dispersed in 100 mL distilled water and in PBS respectively, by intense sonication at 50% amplitude for 1 h. The as resulted colloidal suspensions were termed SM2-T/W and SM2-T/PBS (Fig. 2).

2.3. Characterization techniques

2.3.1. Powder X-ray diffraction (XRD)

The phase composition of the naked nanopowders was investigated by X-ray diffraction (XRD) using a Rigaku Ultima IV diffractometer (monocromated CuKα radiation) (Tokyo, Japan), operating at 40 kV and 40 mA. The following PDF and COD files were used for peak assignment: PDF-330664 (hematite, α-Fe_2O_3), PDF-391346 (maghemite, γ-Fe_2O_3), PDF-190629 (magnetite, Fe_3O_4), COD-1011198 (wuestite, FeO), COD-9015330 and COD-9006603 (iron, Fe).

The average crystallite size of the major phase was calculated using the PDXL 2.0 software based on the XRD patterns by the Sherrer's equation, described below:

$$D_{XRD} = \frac{0.9 \cdot \lambda}{\beta \cdot \cos\theta} \quad (1)$$

Where: D_{XRD}—the crystallites size (nm), λ—radiation wavelength (CuKα, 0.15406 nm), β—the full width at half of the maximum (radians), θ—the Bragg-angle.

The peaks used for the Fe_3O_4 and γ-Fe_2O_3 crystallite size calculation were the one corresponding to 311 and 440 hkl planes. The percentage of crystalline phases was estimated based on the XRD patterns using the relative intensity ratio (RIR) method.

2.3.2. Thermal behavior

Thermal behavior of the iron oxides nanopowders was studied over the temperature range of 25–1000 °C using a Netzsch STA 449C (Selb-Bavaria, Germany) instrument, equipped with alumina crucibles. The thermogravimetric (TG) and the differential scanning calorimetry (DSC) curves were recorded at a heating rate of 10 $K \cdot min^{-1}$ under dynamic air atmosphere at a flow rate of 20 $mL \cdot min^{-1}$.

2.3.3. Specific surface area and adsorption-desorption isotherms

In order to measure the specific surface area of both nanopowders (M1 and M2), S_{BET}, it was employed the Brunauer, Emmett, Teller (BET) nitrogen gas adsorption technique using a Micromeritics ASAP 2020 instrument (Norcross, GA, USA). Considering that the magnetic nanoparticles have spherical shape and using the Eq. (2) the equivalent diameter can be calculated:

$$D_{BET} = \frac{6000}{\rho \cdot S_{BET}} \quad (2)$$

Where: D_{BET} – the grain size (nm), — the theoretical density of magnetic nanoparticles, S_{BET} – the BET surface area (m^2/g).

2.3.4. Magnetization measurements

The magnetic measurements of both naked nanopowders were performed at room temperature on a vibrating sample magnetometer, Lake Shore VSM-system 7404 (Westerville, Ohio, USA).

2.3.5. Transmission and scanning electron microscopy

The morphology and size of both (M1 and M2) naked nanopowders were characterized by scanning electron microscopy (SEM), energy dispersive X-ray (EDX) and transmission electron microscopy (TEM) using a Hitachi HD2700 cold field emission STEM (Chiyoda, Tokyo, Japan) with two windowless EDX detectors from Oxford Instruments (UK). The morphology of colloidal suspensions obtained by coating the M2 nanopowder with OA and Tween 80 and dispersed in various liquid medium, was investigated by transmission electron microscopy (TEM).

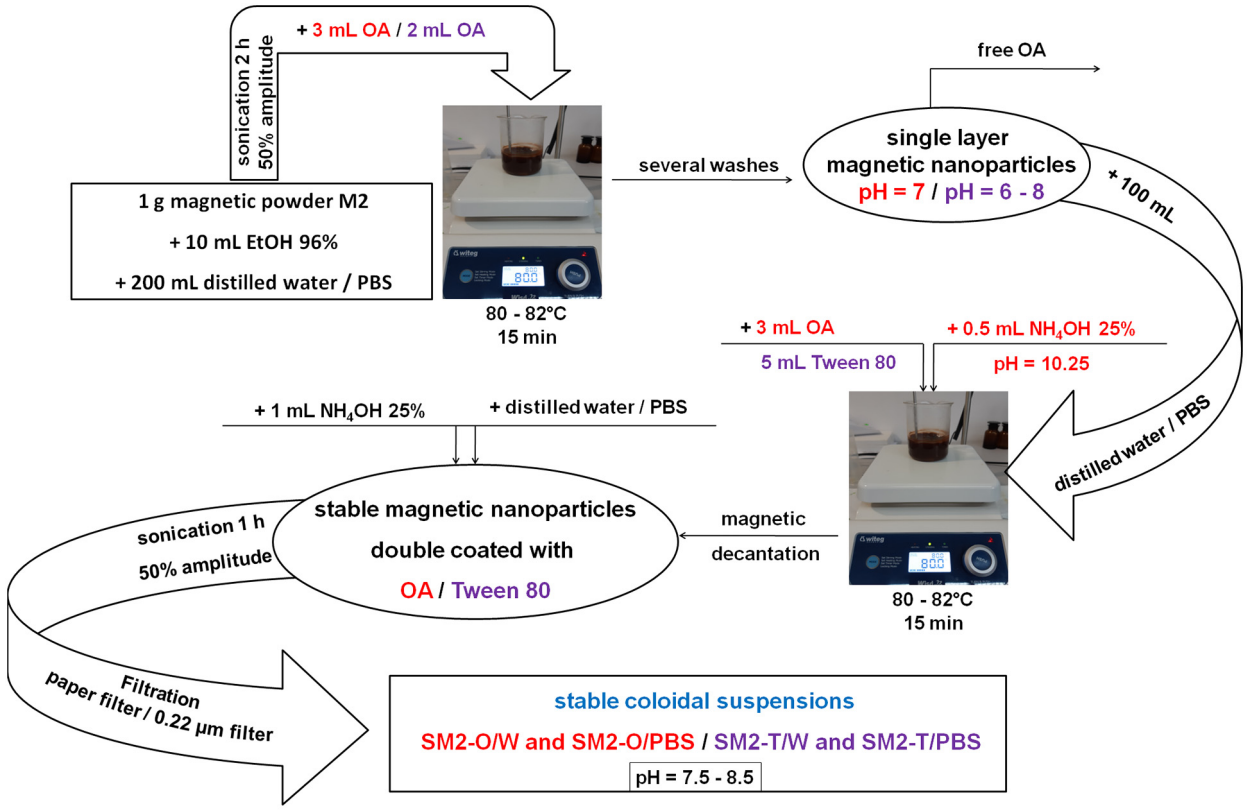

Fig. 2. Schematic protocol of stable colloidal suspensions preparation; M2 magnetic nanoparticles stabilized with OA/Tween 80, dispersed in distilled water (sample SM2-O/W; SM2-T/W) and PBS (sample SM2-O/PBS; SM2-T/PBS) respectively.

2.3.6. Dynamic light scattering and zeta potential

The hydrodynamic diameter (Dh), polydispersity index (PDI) and zeta potential were measured by dynamic light scattering using a Delsa Nano C particle analyzer from Beck-man Coulter (Brea, CA, USA). This analyzer uses photon correlation spectroscopy and measures the particle size of samples in suspension in a range from 0.6 nm to 7 µm. Zeta potential was measured by an electrophoretic light scattering technique using a flow cell.

3. Results and discussion

3.1. XRD, thermal behavior and adsorption-desorption isotherms of magnetic nanopowders

This work is focused on the preparation of magnetic iron oxides, that have the characteristics required in biomedical applications, by the solution combustion synthesis using conventional and microwave ignition respectively. Foremost, a comprehensive analysis of the iron oxide nanoparticles characteristics induced by the ignition of the combustion reactions using microwave and conventional ignition was performed. The synthesis conditions and structural characteristics of the nanopowders M1 and M2 are shown in Table 1.

Manikandan et al. [49] have obtained Fe_3O_4 nanoparticles by microwave ignition of the solution combustion synthesis. They used $Fe(NO_3)_3 \cdot 9H_2O$, urea ($CO(NH_2)_2$) as fuel and a household microwave-oven operating at 850 W. Radpour et al. [55] studied the microwave-assisted solution combustion synthesis of Fe_3O_4 powders using ferric nitrate nonahydrate and citric acid as fuel in the presence of ammonia (NH_4OH) solution. They have used a household microwave-oven operating at 750 W.

In our work we have used also ferric nitrate nonahydrate as oxidizer and citric acid as fuel but we propose a more simple experimental procedure without NH_4OH and by using an equipment operating at 800 W which ensures the external elimination of the resulting gases during the reaction (Fig. 1-B).

3.1.1. XRD characterization

The phase composition of the synthesized nanopowders (M1 and M2) was investigated by X-ray diffraction and the XRD patterns are shown in Fig. 3.

The phase composition of both M1 and M2 nanopowders presented in Table 1 was established by the PDXL2 software, based on the X-ray diffraction patterns (Fig. 3), using the RIR method. It can be noticed that the ignition procedure significantly influences the phase composition of the combustion reaction products. In case of sample M1 the main phase is magnetite (97%) alongside with maghemite (3%) while the main phase of sample M2 is maghemite (85%) alongside with magnetite (11%), wüstite (2%) and Fe (2%). It can be also observed the sharper profile of the diffraction peaks of sample M1 as compared to sample M2. This indicates that by the ignition of combustion reaction using a heating mantle (conventional heating) results a much better crystallized powder (M1) in comparison with the one prepared in microwave oven (M2).

Another difference between the two samples is the average crystallite size of the major phase, (D_{XRD}) calculated from the XRD pattern (Table 1). The mean crystallite size of sample M1 (23 nm), using a heating mantle, is more than 4 times larger compared to sample M2 (5 nm), prepared in microwave oven, which could be due to the higher temperature developed during the combustion reaction ignited in the heating mantle. Our results are consistent with the results reported by Manikandan et al. [49].

The characterization of the two types of magnetic nanoparticles M1 and M2 in terms of phase composition, demonstrated that the ignition of combustion reactions using conventional heating results in a much

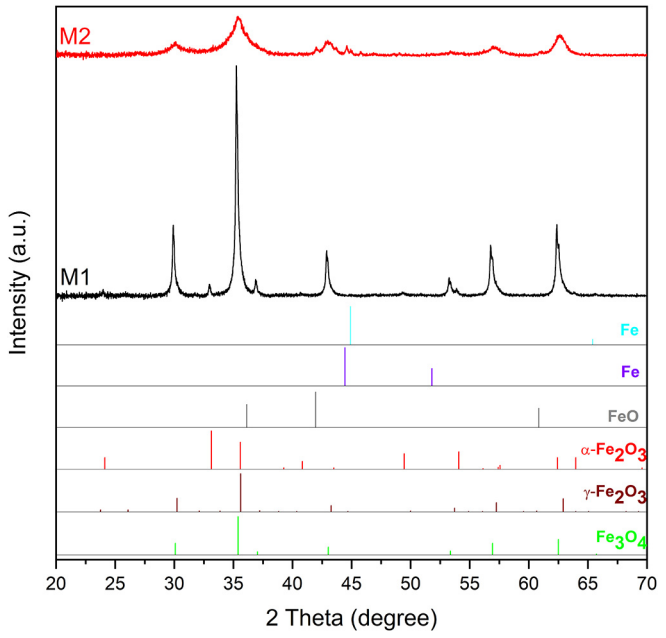

Fig. 3. XRD patterns of nanopowders M1 and M2, compared to the XRD patterns of α-Fe_2O_3 (PDF-330664), γ-Fe_2O_3 (PDF-391346), Fe_3O_4 (PDF-190629), FeO (COD-1011198), Fe (COD-9015330, COD-9006603) from the International Centre for Diffraction Data Powder Diffraction File (ICDD PDF) 4+ 2019 and Crystallographic Open Database (COD) data.

better crystallized powder (M1) in comparison with the one prepared by microwave heating (M2). On the other hand, these results are in disagreement with the ones stated by Radpour et al. [53,55] who reported a little bit higher value of the crystallite size for the Fe_3O_4 particles prepared by microwave ignition as compared to that prepared by conventional ignition of the solution combustion reaction.

The mean crystallite size of sample M2 is more suitable for biomedical applications, considering that the extremely small sizes of magnetic iron oxide nanoparticles ($d < 4$ nm) can be used as T1 magnetic resonance imaging (MRI) contrast agents, whereas magnetic nanoparticles with size of 10 nm are more efficient T2 MRI contrast agents [60]. This result confirms that the reaction conditions and the equipment we have used for the microwave ignition of the combustion reaction is appropriate to provide magnetic nanoparticles suitable for biomedical applications.

The XRD results are in agreement with those obtained by Predescu et al. [61], who observed a single major intensity peak at 35.28° for magnetite in dextran coated magnetite nanoparticles and with the data obtained by Yew et al. [62] and Basavegowda et al. [63].

3.1.2. Thermal analysis

The thermal behavior of samples M1 and M2 is shown in Fig. 4. The small endothermic effect on DSC curve at about 100 °C, accompanied by mass loss on TG curve of both powders is attributed to water evaporation in the samples. The DSC curves of both samples exhibit a large exothermic effect, between 150 and 450 °C for sample M1 and between 200 and 400 °C for sample M2. The exothermic effect of sample M1 is broader as compared to that of sample M2. This can be explained by the overlapping of two exothermic effects in case of sample M1-a weak one assigned to the oxidation of magnetite (which is the main phase in sample M1) to maghemite, accompanied by mass gain on TG curve (0.58%) and a stronger one assigned to the oxidative degradation of the organic residue resulting from the combustion reaction and accompanied by mass loss on TG curve (2.94%).

The TG curve of nanopowder M2 does not exhibit the mass increase between 200 and 400 °C which is in accordance with the presence of maghemite as main phase in this sample (Table 1). The exothermic effect evidenced on the DSC curve of sample M2 is assigned to the oxidative degradation of the organic residue resulting from the combustion reaction. The mass loss of 9.19% on the TG curve of sample M2 is much higher compared to the 2.94% in case of sample M1 which demonstrates the higher content of organic residue in the sample M2 prepared in microwave oven. This organic residue creates a reducing atmosphere in the system favoring the formation of low amount of FeO and Fe in case of sample M2, confirmed by the phase composition (Table 1), which could explain the mass increase of 1.06% between 400 and 550 °C and attributed to the FeO and Fe oxidation. The small exothermic effect located around 500 °C may be assigned to the maghemite to hematite polymorph transformation.

The TG-DSC results obtained by thermal analysis for both magnetic samples obtained by com-bustion reactions using microwave and conventional heating (Fig. 4) are in accordance with their phase composition revealed by XRD analysis. As shown from XRD-RIR analysis, sample M1 has a high content of magnetite (Fe_3O_4). Many studies [64–66] demonstrated the high tendency of magnetite to oxidation in air at low temperatures. It has been proved [65,66] that, by heating in air, magnetite pass through two distinct stages characterized by exothermic effects: the first stage (starting at about 200 °C) is due to the oxidation of magnetite to maghemite and the second one (starting at about 375 °C) to the polymorph transformation of maghemite to hematite. It has also been demonstrated that the thermal stability of magnetite depends mostly on the grain size, the rate of oxidation, and on the synthesis procedure [65,67]. The thermal behavior of M1 sample is in agreement with the literature reports presented above. The oxidation of magnetite to maghemite is evidenced by the mass gain on TG curve and the exothermic effect on DSC curve at about 250 °C, which overlaps with a much stronger effect at around 355 °C. The

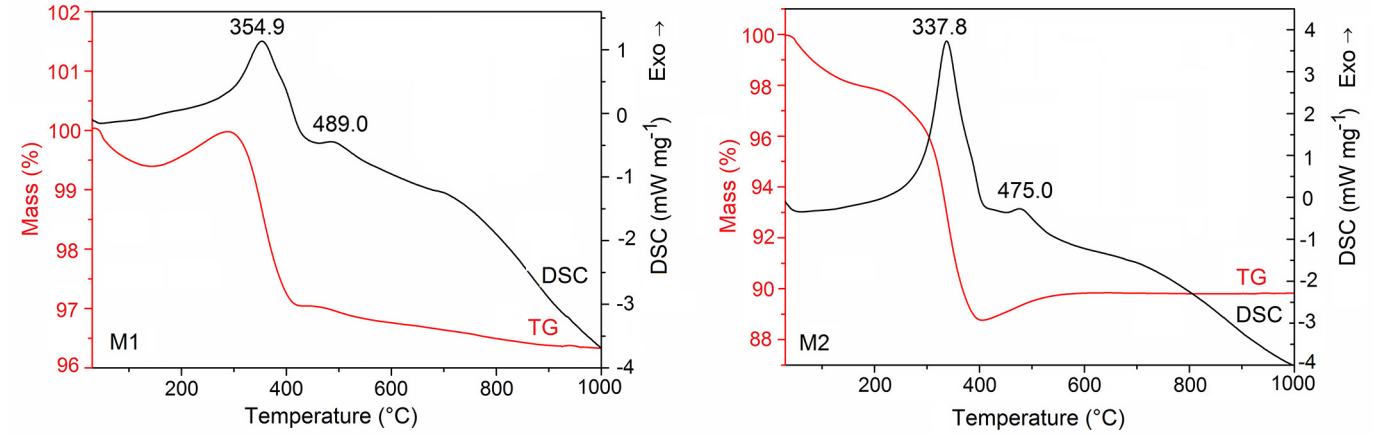

Fig. 4. TG/DSC curves of nanopowders M1 and M2.

exothermic process, evidenced on DSC curve at 489 °C corresponds to the transition of maghemite (γ-Fe_2O_3) to hematite (α-Fe_2O_3) [68,69]. Unlike M1, the main phase of sample M2 is maghemite (85%) alongside with magnetite (11%), and minor amounts of wüstite (2%) and Fe (2%) (Table 1) such that the TG curve does not show the mass increase at about 200–250 °C. In the same time the strong exothermic effect evidenced on DSC curve at 337.8 °C is less wide in comparison to that exhibited on DSC curve of sample M1 at 354.9 °C. In case of sample M2 can be observed the mass increase of 1.06% between 400 and 550 °C that can be attributed to the FeO and Fe oxidation. The exothermic effect evidenced on DSC curve at 475 °C, hides both the oxidation process of FeO and Fe as well as the polymorph transformation of maghemite to hematite. In accordance with the literature reports [47,70,71], the two strong exothermic effects on DSC curve of sample M1 (354.9 °C) and sample M2 (337.8 °C), are assigned to the combustion of the fuel residual carbonaceous species.

3.1.3. Specific surface area and adsorption-desorption isotherms

The N_2 adsorption-desorption isotherms and pore size distribution of nanopowders M1 and M2 are shown in Fig. 5.

It can be observed the practically similar shape of the two isotherms (Fig. 5-A) which are of type II with H3 hysteresis loop, according to IUPAC classification. Regarding the pore size distribution (Fig. 5-B), it can be noticed that both samples exhibit meso-pores. While nanopowder M2 shows only mesopores with diameters between 3 and 6 nm, in case of sample M1 alongside pores with diameters between 3 and 4.5 can be also observed pores with diameter between 4.5 and 11 nm. These results are in accordance with the higher average pore diameter of sample M1 as compared with that of sample M2 (Table 1).

It is important to notice (Table 1) the larger specific surface area of sample M2 (70.71 m^2/g) as compared to that of sample M1 (41.53 m^2/g). This result is in agreement with the smaller crystallite size of sample M2 obtained in the microwave oven by comparison to sample M1.

The specific surface area represents an important characteristic of nanomaterials. High values of the specific surface area are essential for many uses of nanomaterials as adsorbents, catalysts as well in the biomedical applications. It can be noticed (Table 1) that the ignition procedure of the combustion reactions considerably influenced the specific surface area of the samples. The specific surface area of sample M2 prepared by microwave ignition is much larger (S_{BET} = 70.71 m^2/g) as compared to that of sample M1 prepared by conventional ignition (S_{BET} = 41.53 m^2/g).

This result is in agreement with the lower synthesis temperature confirmed by the XRD analysis. In the case of conventional ignition, the specific surface area reported by us (S_{BET} = 41.53 m^2/g) and by Manikandan et al. [49] (S_{BET} = 37.95 m^2/g) are in good accordance but both are different to the one reported by Radpur et al. [55] (S_{BET} = 71.50 m^2/g) for the synthesis of Fe_3O_4. The high value of the specific surface area of sample M2, prepared by microwave ignition, recommends it for biomedical applications.

3.2. Magnetic properties evaluation

According to the literature [49,71–73], many factors affect the magnetic properties of materials such as phase composition, crystallinity, particle size and morphology, crystallite size as well as the carbon content. The effect of the ignition procedure of the combustion reaction on the magnetic properties of the samples M1 and M2 is shown in Fig. 6.

The hysteresis loops of the M1 and M2 nanopowders (Fig. 6), recorded at room temperature evidence zero remanence and coercivity which prove the superparamagnetic behavior of both samples. By comparing the saturation magnetization of the two samples, a higher value can be noticed in the case of sample M1 (66.6 emu/g) prepared in the heating mantle by conventional heating. The lower value of the saturation magnetization of sample M2 (41.8 emu/g), prepared in microwave oven, is expected considering the different phase composition (Table 1) and the higher content of non-magnetic organic residue.

The lower value of the saturation magnetization of sample M2 (41.8 emu/g), prepared by microwave ignition, can be explained by the smaller size of maghemite particles, larger specific surface area and higher content of non-magnetic organic residue by comparison to sample M1 (66.6 emu/g) prepared via conventional ignition. The saturation magnetization of both samples, M1 and M2 (Fig. 6) are in accordance with the data from the study conducted by Aliramaji and co-workers [74] and much better compared with the study conducted by Yadav and co-workers [75].

3.3. Size, morphology and structural analysis

3.3.1. Size, morphology and structural analysis of naked nanopowders M1 and M2

The results of the SEM-TEM-EDX analyses of the nanopowders M1 and M2 are shown in Fig. 7.

The SEM image of sample M1 (Fig. 7-A) reveals aggregated particles which is explained by the higher temperature developed by the reaction ignition in the heating mantle. The SEM image of sample M2 (Fig. 7-E) evidences smaller particles, yet also agglomerated.

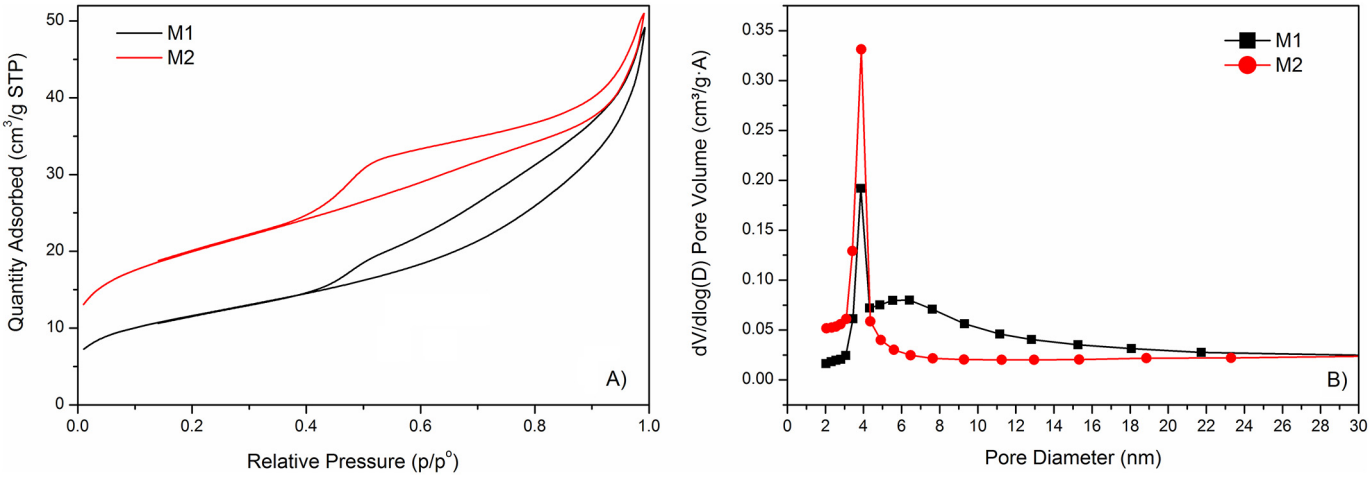

Fig. 5. N_2 adsorption-desorption isotherms (A) and pore size distribution (B) of nanopowders M1 and M2.

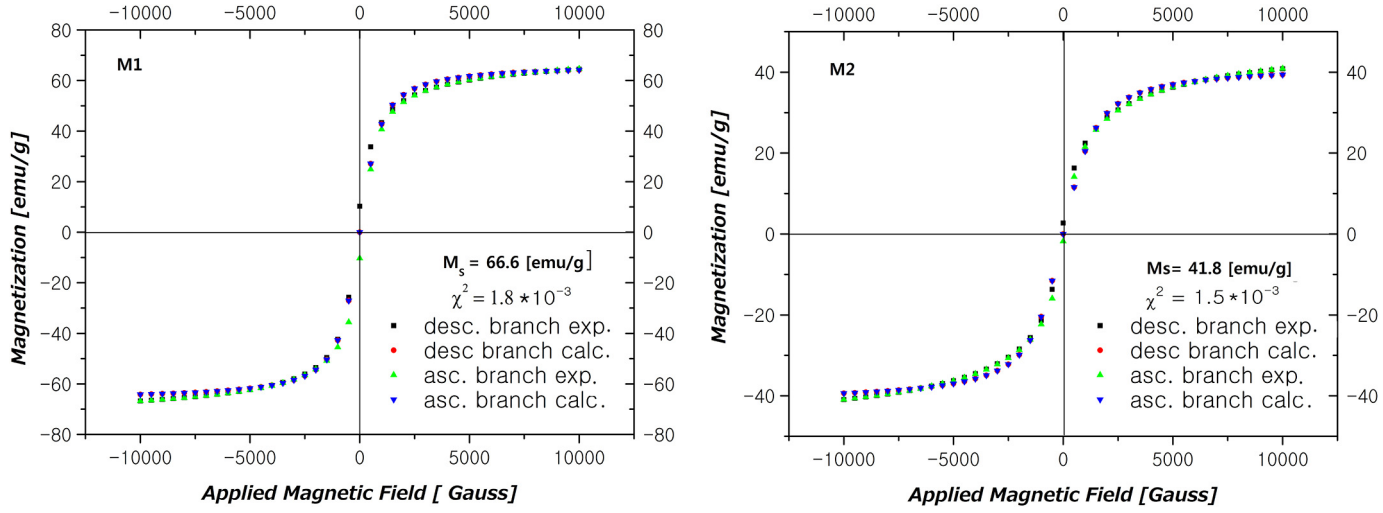

Fig. 6. Magnetization curves of nanopowders M1 and M2.

The EDX spectrum and elemental distribution of sample M2 (Fig. 7-G and 7-H) demonstrates the higher content of carbon as compared to sample M1 (Fig. 7-C and 7-D), in agreement with the TG results. The EDX mapping reveals that M1 product is homogenous throughout the aggregate, but less so for M2, and that both have an amorphous carbon content.

TEM investigations indicate that M1 nanoparticles, prepared in the heating mantle, have a narrow size distribution, with a peak distribution size at 20 nm, medium size 15.62 ± 4.4 nm (Fig. 7-B). The M2 nanoparticles prepared in the microwave oven have a broader size distribution pattern with a flat peak at 15 nm, medium size 10.66 ± 3.09 nm (Fig. 7-F). In Fig. 8 is depicted the size distribution of the particles as a function of frequency, of both M1 and M2 nanopowders. The values recorded are in the range of 10–20 nm in the case of M1 nanopowders (Fig. 8-A), and in the range of 7–15 nm in the case of M2 nanopowders (Fig. 8-B), which indicate a high polydispersity of the nanoparticles.

For biomedical applications, besides the crystal structure and crystallinity of iron oxides nanoparticles, other parameters that should be strictly controlled in the synthesis of these magnetic nanoparticles are shape, size and uniformity. It is known that the heat and gases released during the reaction have a major influence on the morphology of the obtained samples [49,53,76]. As can be seen from the SEM image, the nanoparticles of sample M1 (Fig. 7-A) are agglomerated, which may be due to the sintering effect caused by the high temperature developed by the conventional ignition [49,77]. The na-noparticles of sample M2 are smaller and also agglomerated (Fig. 7-E), probably due to the magnetic interactions among the particles [49,76].

Similar results have been described in the literature by Coricovac et al. [58]; Aliramaji et al. [74]; Yadav et al. [75] and Rivera-Chaverra et al. [78]. According to Gupta and Gupta [19] magnetic nanoparticles with a size range between 10 and 100 nm, perform the most prolonged blood stream circulation time, being the most suitable for intravenous injection. Magnetic nanoparticles smaller than 10 nm are not desired for certain biomedical applications due to the fact that are rapidly removed by renal clearance. Moreover, it was established that the biggest and the smallest nanoparticles seems to be toxic with cell interaction inducing cell death through apoptosis, oxidative stress, DNA destruction and mutagenesis [79]. In the case of non-using capping agent the nanoparticles are showing an inherent tendency to exhibit aggregation (Fig. 7-A and Fig. 7-E). Surface coatings avoid the agglomeration of nanoparticles and provide suitable surface properties [19,80]. Besides the prevention of nanoparticles agglomerations, the role of coatings consist in improvements of stability, as well as to prevent oxidation, corrosion and their toxicity [81].

3.3.2. Morphology and structural analysis of colloidal suspensions

A considerable number of studies refers that for the biomedical applications (diagnostic and therapy) [7,20,82,83] is necessary that the magnetic iron oxide nanoparticles exhibit superparamagnetic behavior at room temperature, biocompatible surface coatings and colloidal stability in aqueous carrier [84]. In the present study the superparamagnetic behavior (Fig. 6) of both magnetic nanopowders was demonstrated, by achieving zero remanence and coercivity at room temperature. Remanent magnetization is a key factor of magnetic nanoparticles for biomedical applications; the more remanence have nanoparti-cles the more they will clump together and block the blood vessels in the human body. Concerning the biocompatible surface coatings and colloidal stability in aqueous carrier, oleic acid (OA) is by far, the most frequently used surfactant. Mainly this is related to its protective capacity to obtained uniform and monodisperse nanoparticles [85], being a skin permeability enhancer, inducing cell death by apoptosis [86]. Various research study showed that the fatty acid played a crucial role in controlling the shape, monodispersity and thermal stability of the iron oxide nanoparticles [87–89].

Between the two magnetic powders, the physicochemical characteristics of M2 nanoparticles proved to be more suitable for biomedical applications (Table 1). Therefore, these nanoparticles were used for the preparation of colloidal suspensions. In order to obtain stable colloidal suspensions, the stabilization of the magnetic nanoparticles must be performed using an optimal surfactant concentration. This optimal concentration gives to the surfactant the ability to de-agglomerate the nanoparticles, thus being an important parameter in the adsorption process. Another important parameter is the alkaline pH in the aqueous phase. An alkaline pH and a fairly high concentration of surfactant, lead to obtaining magnetic nanoparticles with high colloidal stability in aqueous media [90]. In the present study were employed two types of surfactant: a fatty acid (oleic acid - OA) and a non-ionic surfactant (Tween 80 - T). There are few studies in the literature dealing with the preparation and characterization of colloidal suspensions using Tween 80 as surfactant [91] but, as far as we know, none of them uses iron magnetic iron nanoparticles prepared by the solution combustion synthesis.

The TEM analyses of the four colloidal suspensions are shown in Fig. 9. TEM images of the SM2-O/W (M2 magnetic nanoparticles coated with double layer of oleic acid and dispersed in distilled water) and SM2-O/PBS (M2 magnetic nanoparticles coated with double layer of oleic acid and dispersed in PBS) colloidal suspensions appear very similar in both dispersion media (Fig. 9-A and 9-B). The particles are well separated, which means that the OA used as surfactant for covering

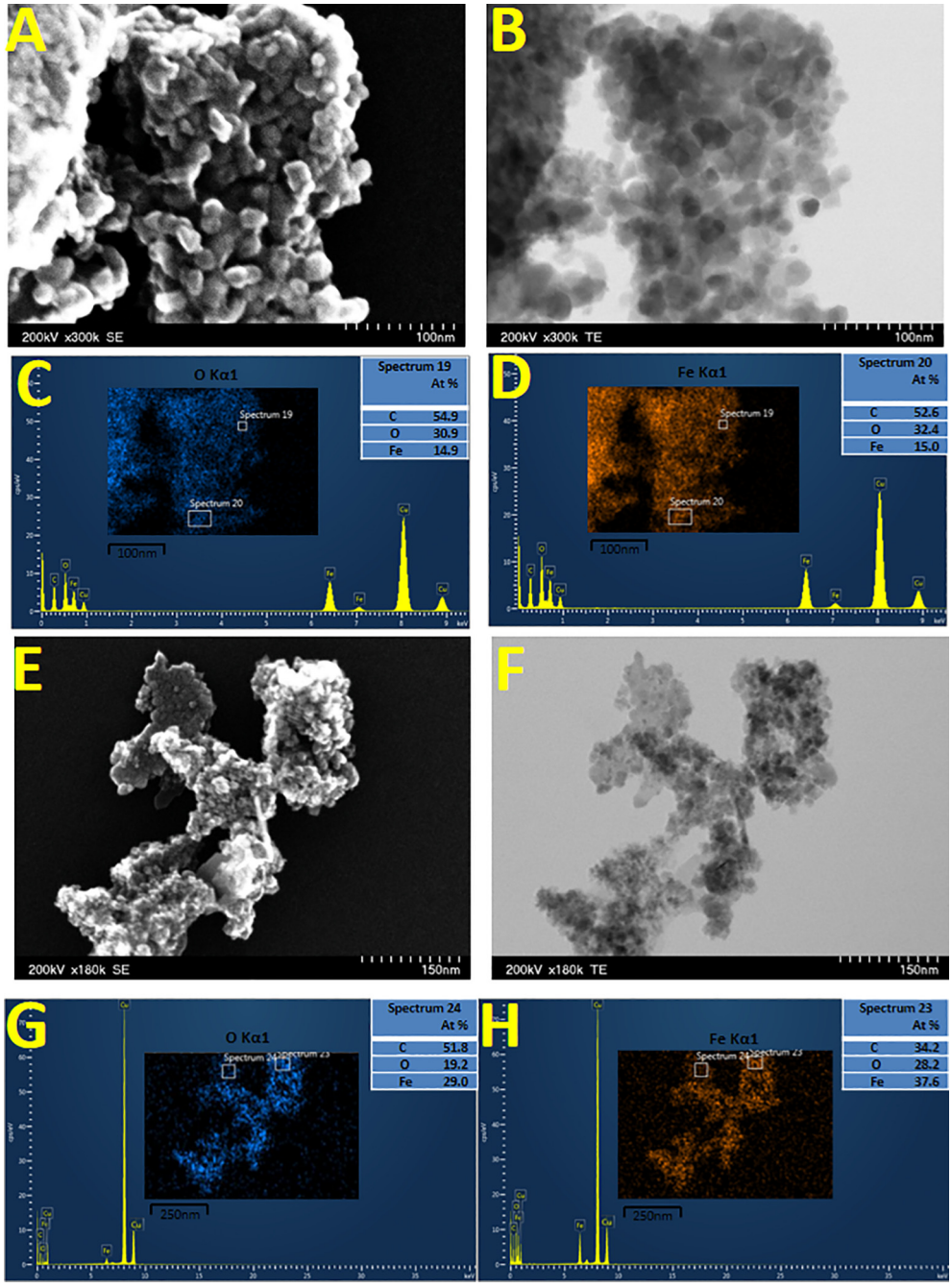

Fig. 7. M1 nanopowder (A - SEM and B – TEM images; C and D – EDX spectrum and elemental distribution), and M2 nanopowder (E - SEM and F – TEM images; G and H – EDX spectrum and elemental distribution).

the magnetic nanoparticles M2 ensures a very good stability, regardless the dispersion medium (distilled water or PBS). TEM images of the SM2-T/W (M2 magnetic nanoparticles coated with oleic acid and Tween 80, dispersed in distilled water) and SM2-T/PBS (M2 magnetic nanoparticles coated with oleic acid and Tween 80, dispersed in PBS) colloidal suspensions also look similar but some agglomerated particles may be noticed (Fig. 9-C and 9-D). This means that Tween 80, which is a nonionic surfactant, does not provide enough repulsions between particles to prevent their agglomerations.

3.4. Dynamic light scattering and zeta potential of colloidal suspensions

In Table 2 are described the results regarding the values of the hydrodynamic diameter, polydispersity index and Zeta potential for all the four colloidal suspensions based on magnetic nanoparticles, coated with surfactants: OA and Tween 80 respectively.

It can be noticed the high stability of the colloidal suspensions provided by the use of OA as surfactant regardless of the dispersion medium, distilled water or PBS, confirmed by the significant negative values of the Zeta potential (−73.98 mV for SM2-O/W and −47.25 mV for SM2-O/PBS). By using Tween 80 as nonionic surfactant are obtained colloidal suspensions which show lower values of Zeta potential (−13.973 mV for SM2-T/W and −11.82 mV for SM2-T/PBS) and consequently, lower stability.

The nature of the dispersion medium, distilled water or PBS, does not significantly influence the stability of the colloidal suspensions. It can be observed only a slight decrease in stability when using PBS as a dispersion medium. It is also noted that the polydispersity index (PDI)

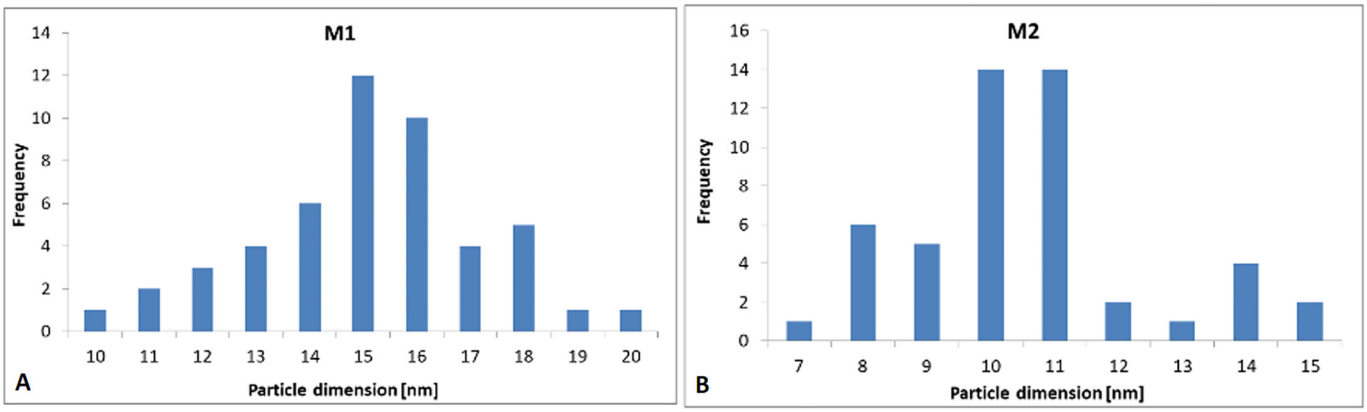

Fig. 8. The frequency distribution of particles size of A – M1 nanopowder and B – M2 nanopowder.

of the four colloidal suspensions has values close to zero which indicates a small polydispersity, so a dimensional homogeneity of the samples.

The data obtained from DLS measurements showed that the values recorded for the size of all colloidal suspensions (Table 2) are in the range of 79–105 nm. The colloidal suspensions termed SM2-O/W and SM2-T/PBS, indicate the presence of good polydispersity (PDI) (Table 2). PDI is a dimensionless parameter that indicates the width of the dimensional distribution of particles. A PDI value closer to zero indicates a lower polydispersity, so a dimensional homogeneity of the sample. The more the PDI tends to 1, the more the polydispersity increases, so the sample is more inhomogeneous in terms of particle size. In general, a sample with a PDI greater than 0.7 indicates an inhomogeneous sample containing aggregates. Our results obtained from PDI measurements showed that the values are in the range of 0.179–0.326. By comparison, the Zeta potential of −73.98 mV for the oleic acid-coated iron oxide nanoparticles dispersed in water (sample SM2-O/W) is much higher than the value of −36 mV reported by Ingram et al. [90] at pH 7 and pH 9 for the same colloidal suspension.

Fig. 10 presents the results recorded for all four colloidal suspensions, in terms of intensity distribution of particles size. It can be observed that all the colloidal suspensions are composed of a single population of nanoparticles (unimodal particle size distribution) with an average hydrodynamic diameter of 91 nm (SM2-O/W – black line); 105 nm (SM2-O/PBS – red line and SM2-T/W – blue line) and 79 nm (SM2-T/PBS – green line). In addition, it can also be seen that in the case of SM2-O/PBS and SM2-T/W colloidal suspensions a broader size distribution of

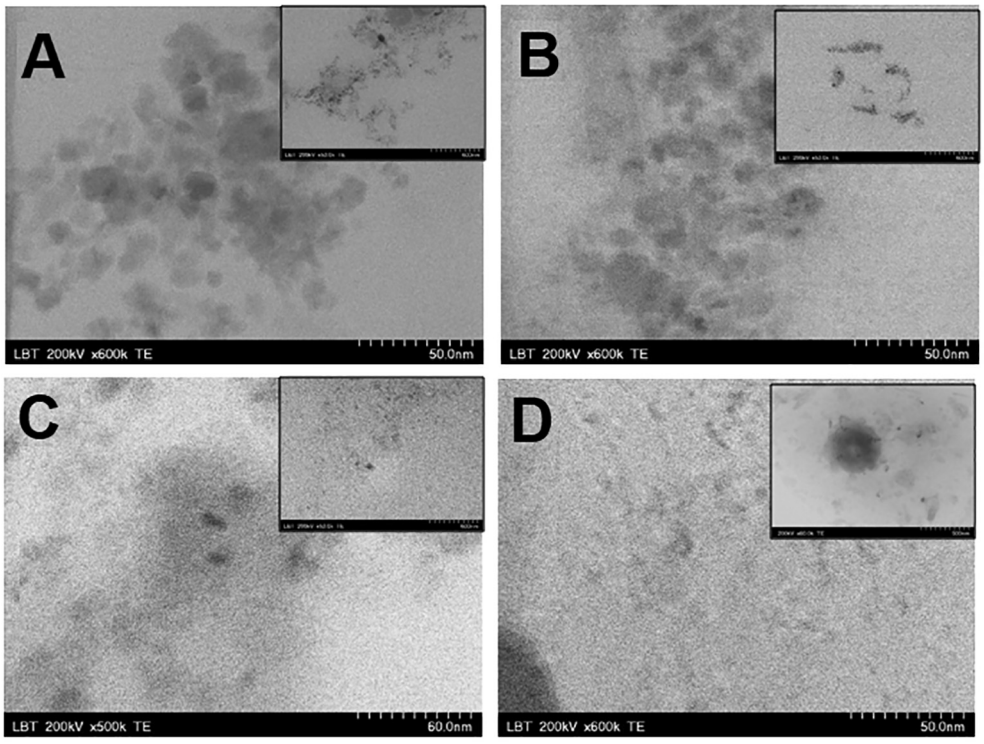

Fig. 9. TEM images of samples: SM2-O/W (A), SM2-O/PBS (B), SM2-T/W (C), and SM2-T/PBS (D). Insets at 50 k magnification, 500 nm scale bar.

Table 2
Characteristics of the colloidal suspensions.

Colloidal suspension	Surfactant	Dispersion medium	Hydrodynamic diameter (nm)	PDI (polydispersity index)	Zeta potential (mV)
SM2-O/W	oleic acid double layer	distilled water	91	0.179	−73.98
SM2-O/PBS	oleic acid double layer	PBS	105	0.326	−47.25
SM2-T/W	oleic acid + tween 80	distilled water	105	0.315	−13.73
SM2-T/PBS	oleic acid + tween 80	PBS	79	0.189	−11.82

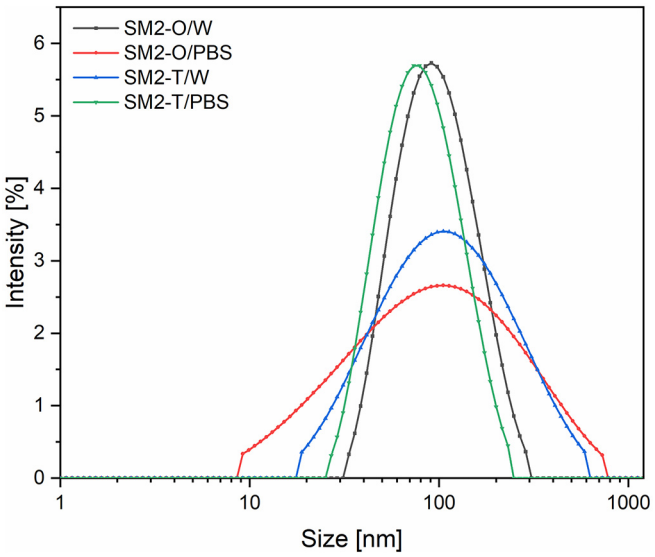

Fig. 10. The intensity distribution of particles size (DLS) of colloidal suspensions.

nanoparticles were obtained while SM2-O/W and SM2-T/PBS colloidal suspensions have a narrower nanoparticles size distribution.

These results together with the small values of the hydrodynamic diameter demonstrate that all the colloidal suspensions have the necessary characteristics to be further tested for biomedical applications.

The results regarding the characteristics of the colloidal suspensions (Table 2) are in agreement with the intensity distribution of particles size (DLS) of colloidal suspensions (Fig. 10), meaning, the samples with narrow size distribution (SM2-O/W and SM2-T/PBS) have low polydispersity index and the samples with broad size distribution (SM2-O/PBS and SM2-T/W) have a slightly higher polydispersity index. This behavior can be explained on the one hand by the liquid carrier (in the case of sample SM2-O/PBS the dispersion medium was PBS as against distilled water) and on the other hand – the use of Tween 80 as nonionic surfactant, with no electrical charge, causing steric repulsion between particles [92]. The values of the Zeta potential (Table 2) evidence that the steric stabilization of the colloidal suspensions provided by Tween 80 is less efficient as compared to the electrosteric stabilization provided by oleic acid [93].

In the end, biomedical applications require stable magnetic nanoparticles in aqueous solutions at neutral pH and physiological conditions. All the data obtained in the current study support the idea that the synthesized colloidal suspensions are suitable candidates for in vivo and in vitro applications for diagnostic or therapeutic purposes.

4. Conclusions

Two magnetic nanopowders were prepared by solution combustion synthesis method using conventional heating and microwave heating. The ignition procedure of the combustion reaction (conventional heating and microwave heating) influences the phase composition and modifies the characteristics of the prepared iron oxide nanoparticles.

Microwave heating leads to a larger specific surface area (70.71 m^2/g), lower saturation magnetization (41.8 emu/g) and lower particle medium size (10.66 ± 3.09 nm), already convenient for various applications. Thermal analyses confirm the presence of some organic residues, resulted from the fuel combustion in case of sample prepared in microwave oven. Magnetic measurements on both magnetic nanopowders confirmed the superparamagnetic behavior of the obtained magnetic nanoparticles.

Water-based or phosphate buffer saline-based colloidal suspensions prepared with iron oxide nanoparticles have good stability and small polydispersity. However, the particles coated with oleic acid exhibit much higher stability compared to those coated with Tween 80, regardless the dispersion medium. The stability of the colloidal suspensions is little influenced by the nature of the dispersion medium. DLS analyses confirmed the nanometric size (an average hydrodynamic diameter range between 79 and 105 nm) what makes them suitable for biomedical applications, in addition to their good stability and solubility in aqueous solutions. All the prepared colloidal suspensions will be further tested for biomedical applications.

Credit authorship contribution statement

Conceptualization: Aylin Capraru and Cornelia Pacurariu; Data curation: Cornelia Pacurariu, Robert Ianos, Radu Lazau, Lucian Barbu-Tudoran; Formal analysis: Aylin Capraru, Elena-Alina Moaca; Funding aquisition: Cornelia Pacurariu; Investigation: Aylin Capraru, Elena-Alina Moaca, Cornelia Pacurariu, Robert Ianos, Radu Lazau, Lucian Barbu-Tudoran; Methodology: Aylin Capraru, Elena-Alina Moaca, Cornelia Pacurariu, Robert Ianos, Radu Lazau, Lucian Barbu-Tudoran; Project administration: Cornelia Pacurariu; Resources: Cornelia Pacurariu; Software: Elena-Alina Moaca, Cornelia Pacurariu, Robert Ianos, Radu Lazau, Lucian Barbu-Tudoran; Supervision: Cornelia Pacurariu, Robert Ianos, Radu Lazau; Validation: Cornelia Pacurariu, Robert Ianos, Radu Lazau; Visualization: Elena-Alina Moaca, Cornelia Pacurariu, Robert Ianos; Writing - original draft: Aylin Capraru, Elena-Alina Moaca, Cornelia Pacurariu; Writing - review & editing: Elena-Alina Moaca, Cornelia Pacurariu, Robert Ianos.

Declaration of Competing Interest

The authors declare that they have no known competing financial interests or personal relationships that could have appeared to influence the work reported in this paper.

Acknowledgments

This research was funded by a grant of Ministery of Research and Innovation, CNCS -UEFISCDI, project number PN-III-P4-ID-PCE-2016-0765, within PNCDI III.

References

[1] A.H. Lu, E.L. Salabas, F. Schüth, Magnetic nanoparticles: synthesis, protection, functionalization and application, Angew. Chem. Int. Ed. 46 (2007) 1222–1224, https://doi.org/10.1002/anie.200602866.

[2] R. Ianoş, C. Păcurariu, S.G. Muntean, E. Muntean, M.A. Nistor, D. Nižňanský, Combustion synthesis of iron oxide/carbon nanocomposites, efficienta dsorbents for anionic and cationic dyes removal from wastewaters, J. Alloys Compd. 741 (2018) 1235–1246, https://doi.org/10.1016/j.jallcom.2018.01.240.

[3] C. Păcurariu, O. Paşka, R. Ianoş, S.G. Muntean, Effective removal of methylene blue from aqueous solution using a new magnetic iron oxide nanosorbent prepared by combustion synthesis, Clean Techn. Environ. Policy 18 (2016) 705–715, https://doi.org/10.1007/s10098-015-1041-7.

[4] R.Y. Hong, J.H. Li, J.M. Qu, L.L. Chen, H.Z. Li, Preparation and characterization of magnetite/dextran nanocomposite used as a precursor of magnetic fluid, Chem. Eng. J. 150 (2009) 572–580, https://doi.org/10.1016/j.cej.2009.03.034.

[5] S. Laurent, D. Forge, M. Port, A. Roch, C. Robic, L.V. Elst, R.N. Muller, Magnetic iron oxide nanoparticles: synthesis, stabilization, vectorization, physicochemical characterizations and biological applications, Chem. Rev. 108 (2008) 2064–2110, https://doi.org/10.1021/cr068445e.

[6] S. Laurent, J.L. Bridot, L.V. Elst, R.N. Muller, Magnetic iron oxide nanoparticles for biomedical applications, Future Med. Chem. 2 (2010) 427–449, https://doi.org/10.4155/fmc.09.164.

[7] L. Mohammed, H.G. Gomaa, D. Ragab, J. Zhu, Magnetic nanoparticles for environmental and biomedical applications: a review, Particuology 30 (2017) 1–14, https://doi.org/10.1016/j.partic.2016.06.001.

[8] P. Xu, G.M. Zeng, D.L. Huang, C.L. Feng, S. Hu, M.H. Zhao, C. Lai, Z. Wei, C. Huang, G.X. Xie, Z.F. Liu, Use of iron oxide nanomaterials in wastewater treatment: a review, Sci. Total Environ. 424 (2012) 1–10, https://doi.org/10.1016/j.scitotenv.2012.02.023.

[9] H. Urreta, G. Aguirre, P. Kuzhir, L.N. López de Lacalle, Seals based on magnetic fluids for high precision spindles of machine tools, Int. J. Precis. Eng. Manuf. 19 (4) (2018) 495–503, https://doi.org/10.1007/s12541-018-0060-9.

[10] S. Parveen, R. Misra, S.K. Sahoo, Nanoparticles: a boon to drug delivery, therapeutics, diagnostics and imaging, Nanomedicine 8 (2012) 147–166, https://doi.org/10.1016/j.nano.2011.05.016.

[11] L.H. Reddy, J.L. Arias, J. Nicolas, P. Couvreur, Magnetic nanoparticles: design and characterization, toxicity and biocompatibility, pharmaceutical and biomedical applications, Chem. Rev. 112 (11) (2012) 5818–5878, https://doi.org/10.1021/cr300068p.

[12] M. Mahmoudi, H. Hofmann, B. Rothen-Rutishauser, A. Petri-Fink, Assessing the in vitro and in vivo toxicity of superparamagnetic iron oxide nanoparticles, Chem. Rev. 112 (2012) 2323–2338, https://doi.org/10.1021/cr2002596.

[13] M. Mahmoudi, S. Sant, B. Wang, S. Laurent, T. Sen, Superparamagnetic iron oxide nanoparticles (SPIONs): development, surface modification and applications in chemotherapy, Adv. Drug Deliv. Rev. 63 (2011) 24–46, https://doi.org/10.1016/j.addr.2010.05.006.

[14] J.E. Rosen, L. Chan, D.B. Shieh, F.X. Gu, Iron oxide nanoparticles for targeted cancer imaging and diagnostics, Nanomedicine 8 (3) (2012) 275–290, https://doi.org/10.1016/j.nano.2011.08.017.

[15] Z. Luo, H. Du, Prospect of different types of magnetic nanoparticles in stem cell therapy, Stem Cell Rev. 16 (4) (2020) https://doi.org/10.1007/s12015-020-09966-9.

[16] S. Xie, B. Zhang, L. Wang, J. Wang, X. Li, G. Yang, Superparamagnetic iron oxide nanoparticles coated with different polymers and their MRI contrast effects in the mouse brains, Appl. Surf. Sci. 326 (2015) 32–38, https://doi.org/10.1016/j.apsusc.2014.11.099.

[17] C. Sun, J.S. Lee, M. Zhang, Magnetic nanoparticles in MR imaging and drug delivery, Adv. Drug Deliv. Rev. 60 (2008) 1252–1265, https://doi.org/10.1016/j.addr.2008.03.018.

[18] F. Scherer, M. Anton, U. Schillinger, J. Henke, C. Bergemann, A. Kruger, B. Gansbacher, C. Plank, Magnetofection: enhancing and targeting gene delivery by magnetic force in vitro and in vivo, Gene Ther. 9 (2002) 102–109, https://doi.org/10.1038/sj.gt.3301624.

[19] A.K. Gupta, M. Gupta, Synthesis and surface engineering of iron oxide nanoparticles for biomedical applications, Rev. Biomater. 26 (2005) 3995–4021, https://doi.org/10.1016/j.biomaterials.2004.10.012.

[20] M.G.M. Schneider, V.L. Lassalle, Magnetic iron oxide nanoparticles as novel and efficient tools for atherosclerosis diagnosis, Biomed. Pharmacother. 93 (2017) 1098–1115, https://doi.org/10.1016/j.biopha.2017.07.012.

[21] J. Kudr, Y. Haddad, L. Richtera, Z. Heger, M. Cernak, V. Adam, O. Zitka, Magnetic nanoparticles: from design and synthesis to real world applications, Nanomaterials 7 (2017) 243, https://doi.org/10.3390/nano7090243.

[22] W. Wu, Z. Wu, T. Yu, C. Jiang, W.S. Kim, Recent progress on magnetic iron oxide nanoparticles: synthesis, surface functional strategies and biomedical applications, Sci. Technol. Adv. Mater. 16 (2015), 023501 https://doi.org/10.1088/1468-6996/16/2/023501.

[23] K. Petcharoen, A. Sirivat, Synthesis and characterization of magnetite nanoparticles via the chemical co-precipitation method, Mater. Sci. Eng. B Solid State Mater. Adv. Technol. 177 (5) (2012) 421–427, https://doi.org/10.1016/j.mseb.2012.01.003.

[24] A. Sirivat, N. Paradee, Facile synthesis of gelatin-coated Fe_3O_4 nanoparticle: effect of pH in single-step co-precipitation for cancer drug loading, Mater. Des. 181 (2019) 107942, https://doi.org/10.1016/j.matdes.2019.107942.

[25] A. Gholizadeh, A comparative study of physical properties in Fe3O4 nanoparticles prepared by coprecipitation and citrate methods, J. Am. Ceram. Soc. 100 (8) (2017) 3577–3588, https://doi.org/10.1111/jace.14896.

[26] J. Wang, J. Sun, Q. Sun, Q. Chen, One-step hydrothermal process to prepare highly crystalline Fe_3O_4 nanoparticles with improved magnetic properties, Mater. Res. Bull. 38 (2003) 1113–1118, https://doi.org/10.1016/S0025-5408(03)00129-6.

[27] R. Das, J.A. Cardarelli, M.H. Phan, H. Srikanth, Magnetically tunable iron oxide nanotubes for multifunctional biomedical applications, J. Alloys Compd. 789 (2019) 323–329, https://doi.org/10.1016/j.jallcom.2019.03.024.

[28] Y. Zhang, Y. Jia, A facile precursor calcination approach to iron oxide micro/nanostructures with a high magnetization, J. Alloys Compd. 659 (2016) 66–73, https://doi.org/10.1016/j.jallcom.2015.11.029.

[29] M. Darbandi, F. Stromberg, J. Landers, N. Reckers, B. Sanyal, W. Keune, H. Wende, Nanoscale size effect on surface spin canting in iron oxide nanoparticles synthesized by the microemulsion method, J. Phys. D 45 (2012) 195001, https://doi.org/10.1088/0022-3727/45/19/195001.

[30] C. Okoli, M. Sanchez-Dominguez, M. Boutonnet, S. Järås, C. Civera, C. Solans, G.R. Kuttuva, Comparison and functionalization study of microemulsion-prepared magnetic iron oxide nanoparticles, Langmuir 28 (2012) 8479–8485, https://doi.org/10.1021/la300599q.

[31] R.A. Mukh-Qasem, A. Gedanken, Sonochemical synthesis of stable hydrosol of Fe_3O_4 nanoparticles, J. Colloid Interface Sci. 284 (2) (2005) 489–494, https://doi.org/10.1016/j.jcis.2004.10.073.

[32] E.H. Kim, H.S. Lee, B.K. Kwak, B.K. Kim, Synthesis of ferrofluid with magnetic nanoparticles by sonochemical method for MRI contrast agent, J. Magn. Magn. Mater. 289 (2005) 328–330, https://doi.org/10.1016/j.jmmm.2004.11.093.

[33] R. Hufschmid, H. Arami, R.M. Ferguson, M. Gonzales, E. Teeman, L.N. Brush, N.D. Browning, K.M. Krishnan, Synthesis of phase-pure and monodisperse iron oxide nanoparticles by thermal decomposition, Nanoscale 7 (2015) 11142–11154, https://doi.org/10.1039/C5NR01651G.

[34] S.W. Lee, J.S. Yoon, S. Kang, K. Kwon, K.S. Chang, S.G. Lee, S.I. Choi, J.R. Jeong, G. Lee, K.M. Nam, Sustainable method for the large scale preparation of Fe_3O_4 nanocrystals, J. Am. Ceram. Soc. 99 (8) (2016) 2578–2584, https://doi.org/10.1111/jace.14262.

[35] C. Pascal, J.L. Pascal, F. Favier, M.L. Elidrissi Moubtassim, C. Payen, Electrochemical synthesis for the control of γ-Fe2O3 nanoparticle size. Morphology, microstructure, and magnetic behavior, Chem. Mater. 11 (1999) 141–147.

[36] E. Mazarío, A. Mayoral, E. Salas, N. Menéndez, P. Herrasti, J. Sánchez-Marcos, Synthesis and characterization of manganese ferrite nanoparticles obtained by electrochemical/chemical method, Mater. Des. 111 (2016) 646–650.

[37] R. Ianos, R. Babuta, C. Pacurariu, R. Lazau, R. Istratie, C. Butaciu, Combustion synthesis of $ZnAl_2O_4$ powders with tuned surface area, Ceram. Int. 43 (12) (2017) 8975–8981, https://doi.org/10.1016/j.ceramint.2017.04.038.

[38] R. Ianos, R. Istratie, C. Pacurariu, R. Lazau, Solution combustion synthesis of strontium aluminate, $SrAl_2O_4$, powders: sin-gle-fuel versus fuel-mixture approach, Phys. Chem. Chem. Phys. 18 (2) (2016) 1150–1157, https://doi.org/10.1039/C5CP06240C.

[39] B.N. Sherikar, B. Sahoo, A.M. Umarji, One-step synthesis of diopside ($CaMgSi_2O_6$) ceramic powder by solution combustion method, Adv. Powder Technol. 31 (8) (2020) 3492–3499, https://doi.org/10.1016/j.apt.2020.06.037.

[40] D. Ozer, Z. Ertekin, K. Pekmez, N.A. Oztas, Fuel effects on $Li_2CuP_2O_7$ synthesized by solution com-bustion method for lithium-ion batteries, Ceram. Int. 45 (4) (2019) 4626–4630, https://doi.org/10.1016/j.ceramint.2018.11.151.

[41] N. Betancur-Granados, J.C. Restrepo, J.I. Tobón, O.J. Restrepo-Baena, Dicalcium silicate ($2CaO \cdot SiO_2$) synthesized through flame spray pyrolysis and solution combustion synthesis methods, Ceram. Int. 45 (7) (2019) 9589–9595, https://doi.org/10.1016/j.ceramint.2018.10.073.

[42] R. Ianoş, A. Tăculescu, C. Păcurariu, I. Lazău, Solution combustion synthesis and characterization of magnetite, Fe_3O_4, nanopowders, J. Am. Ceram. Soc. 95 (2012) 2236–2240, https://doi.org/10.1111/j.1551-2916.2012.05159.x.

[43] P. Heidari, S.M. Masoudpanah, Structural and magnetic properties of $MgFe_2O_4$ powders synthesized by solution combustion method: the effect of fuel type, J. Mater. Res. Technol. 9 (3) (2020) 4469–4475, https://doi.org/10.1016/j.jmrt.2020.02.073.

[44] V.D. Sudheesh, N. Thomas, N. Roona, P.K. Baghya, S. Varkey, Synthesis, characterization and influence of fuel to oxidizer ratio on the properties of spinel ferrite (MFe_2O_4, M = Co and Ni) prepared by solution combustion method, Ceram. Int. 43 (17) (2017) 15002–15009, https://doi.org/10.1016/j.ceramint.2017.08.023.

[45] S.G. Muntean, M.A. Nistor, R. Ianos, C. Pacurariu, A. Capraru, V.A. Surdu, Combustion synthesis of Fe3O4/Ag/C nanocomposite and application for dyes removal from multicomponent systems, Appl. Surf. Sci. 481 (2019) 825–837, https://doi.org/10.1016/j.apsusc.2019.03.161.

[46] S. Sharma, N. Choudhary, M.K. Verma, N.D. Sharma, D. Singh, Cation distribution and magnetic properties of nano and bulk $CoCrFeO_4$ ferrite synthesized by glycine-nitrate combustion method, Ceram. Int. 43 (14) (2017) 11083–11089, https://doi.org/10.1016/j.ceramint.2017.05.154.

[47] E. Esmaeili, A. Khodadadi, Y. Mortazavi, Microwave-induced combustion process variables for MgO nanoparticle synthesis using polyethylene glycol and sorbitol, J. Eur. Ceram. Soc. 29 (2009) 1061–1068, https://doi.org/10.1016/j.jeurceramsoc.2008.07.051.

[48] R. Rosa, C. Ponzoni, C. Leonelli, Direct energy supply to the reaction mixture during microwave-assisted hydrothermal and combustion synthesis of inorganic materials, Inorganics 2 (2) (2014) 191–210, https://doi.org/10.3390/inorganics2020191.

[49] A. Manikandan, J. Judith Vijaya, J. Arul Mary, L. John Kennedy, A. Dinesh, Structural, optical and magnetic properties of Fe_3O_4 nanoparticles prepared by a facile microwave combustion method, J. Ind. Eng. Chem. 20 (2014) 2077–2085, https://doi.org/10.1016/j.jiec.2013.09.035.

[50] L.C. Nehru, V. Swaminathan, C. Sanjeeviraja, Rapid synthesis of nanocrystalline ZnO by a microwave-assisted combustion method, Powder Technol. 226 (2012) 29–33, https://doi.org/10.1016/j.powtec.2012.03.042.
[51] V. Vasanthi, A. Shanmugavani, C. Sanjeeviraja, R. Kalai Selvan, Microwave assisted combustion synthesis of $CdFe_2O_4$: magnetic and electrical properties, J. Magn. Magn. Mater. 324 (2012) 2100–2107, https://doi.org/10.1016/j.jmmm.2012.02.018.
[52] A. Manikandan, J. Judith Vijaya, M. Sundararajan, C. Meganathan, L. John Kennedy, M. Bououdina, Optical and magnetic properties of mg-doped $ZnFe_2O_4$ nanoparticles prepared by rapid microwave combustion method, Superlattice. Microst. 64 (2013) 118–131, https://doi.org/10.1016/j.spmi.2013.09.021.
[53] M. Radpour, S. Alamolhoda, S.M. Masoudpanah, Effects of pH value on the microstructure and magnetic properties of solution combusted Fe_3O_4 powders, Ceram. Int. 43 (16) (2017) 13729–13734, https://doi.org/10.1016/j.ceramint.2017.07.085.
[54] M. Sertkol, Y. Köseoğlu, A. Baykal, H. Kavas, A. Bozkurt, M.S. Toprak, Microwave synthesis and characterization of Zn-doped nickel ferrite nanoparticles, J. Alloys Compd. 486 (1–2) (2009) 325–329, https://doi.org/10.1016/j.jallcom.2009.06.128.
[55] S.M. Masoudpanah Radpour, S. Alamolhoda, Microwave-assisted solution combustion synthesis of Fe_3O_4 powders, Ceram. Int. 43 (17) (2017) 14756–14762, https://doi.org/10.1016/j.ceramint.2017.07.216.
[56] N.C.S. Selvam, R.T. Kumar, L.J. Kennedy, J.J. Vijaya, Comparative study of microwave and conventional methods for the preparation and optical properties of novel MgO-micro and nano-structures, J. Alloys Compd. 509 (2011) 9809–9815, https://doi.org/10.1016/j.jallcom.2011.08.032.
[57] L. Zhang, R. He, H.C. Gu, Oleic acid coating on the monodisperse magnetite nanoparticles, Appl. Surf. Sci. 253 (2006) 2611–2617, https://doi.org/10.1016/j.apsusc.2006.05.023.
[58] D.E. Coricovac, E.A. Moacă, I. Pinzaru, C. Cîtu, C. Soica, C.V. Mihali, C. Păcurariu, V.A. Tutelyan, A. Tsatsakis, C.A. Dehelean, Biocompatible colloidal suspensions based on magnetic Iron oxide nanoparticles: synthesis, characterization and toxicological profile, Front. Pharmacol. 8 (2017) 154, https://doi.org/10.3389/fphar.2017.00154.
[59] Y.M. Wang, X. Cao, G.H. Liu, R.Y. Hong, Y.M. Chen, X.F. Chen, H.Z. Li, B. Xu, D.G. Wei, Synthesis of Fe_3O_4 magnetic fluid used for magnetic resonance imaging and hyperthermia, J. Magn. Magn. Mater. 323 (2011) 2953–2959, https://doi.org/10.1016/j.jmmm.2011.05.060.
[60] C. De Montferrand, L. Hu, I. Milosevic, V. Russier, D. Bonnin, L. Motte, A. Brioude, Y. Lalatonne, Iron oxide nanoparticles with sizes, shapes and compositions resulting in different magnetization signatures as potential labels for multiparametric detection, Acta Biomater. 9 (4) (2013) 6150–6157, https://doi.org/10.1016/j.actbio.2012.11.025.
[61] A.M. Predescu, E. Matei, A.C. Berbecaru, C. Pantilimon, C. Drăgan, R. Vidu, C. Predescu, V. Kuncser, Synthesis and characterization of dextran-coated iron oxide nanoparticles, R. Soc. Open Sci. 5 (2018) 171525, https://doi.org/10.1098/rsos.171525.
[62] Y.P. Yew, K. Shameli, M. Miyake, N.B.B. Khairudin, S.E.B. Mohamad, T. Naiki, K.X. Lee, Green biosynthesis of superparamagnetic magnetite Fe_3O_4 nanoparticles and biomedical applications in targeted anticancer drug delivery system: a review, Arab. J. Chem. 13 (2020) 2287–2308, https://doi.org/10.1016/j.arabjc.2018.04.013.
[63] N. Basavegowda, K. Mishra, Y.R. Lee, Sonochemically synthesized ferromagnetic Fe_3O_4 nanoparticles as a recyclable cat-alyst for the preparation of pyrrolo [3,4-c] quinoline-1,3-dione derivatives, RSC Adv. 4 (2014) 61660–61666, https://doi.org/10.1039/C4RA11623B.
[64] K. Haneda, A.H. Morrish, Magnetite to maghemite transformation in ultrafine particles, J. Phys. Colloque Cl 38 (1977) https://doi.org/10.1051/jphyscol:1977166 Cl-321-323.
[65] H. Lepp, Stages in the oxidation of magnetite, Am. Mineral. 42 (9–10) (1957) 679–681.
[66] J.P. Sanders, P.K. Gallagher, Thermomagnetometric evidence of γ-Fe_2O_3 as an intermediate in the oxidation of magnetite, Thermoch. Acta 406 (2003) 241–243, https://doi.org/10.1016/S0040-6031(03)00250-8.
[67] B.K. Szostko, U. Wykowska, D. Satula, P. Nordblad, Thermal treatment of magnetite nanoparticles, Beilstein J. Nanotechnol. 6 (2015) 1385–1396, https://doi.org/10.3762/bjnano.6.143.
[68] X. Ye, D. Lin, Z. Jiao, L. Zhang, The thermal stability of nanocrystalline maghemite Fe_2O_3, J. Phys. D. Appl. Phys. 31 (1998) 2739–2744, https://doi.org/10.1088/0022-3727/31/20/006.
[69] D.E. Fouad, C. Zhang, H. El-Didamony, L. Yingnan, T.D. Mekuria, A.H. Shah, Improved size, morphology and crystallin-ity of hematite (α-Fe_2O_3) nanoparticles synthesized via the precipitation route using ferric sulfate precursor, Results Phys. 12 (2019) 1253–1261, https://doi.org/10.1016/j.rinp.2019.01.005.
[70] R. Ianoș, E.A. Tăculescu (Moacă), C. Păcurariu, D. Niznansky, γ-Fe_2O_3 nanoparticles prepared by combustion synthesis, followed by chemical oxidation of residual carbon with H_2O_2, Mater. Chem. Phys. 148 (2014) 705–711, https://doi.org/10.1016/j.matchemphys.2014.08.038.
[71] R. Ianoș, E.A. Moacă, A. Căpraru, R. Lazău, C. Păcurariu, Maghemite, γ-Fe_2O_3, nanoparticles preparation via carbon-templated solution combustion synthesis, Ceram. Int. 44 (12) (2018) 14090–14094, https://doi.org/10.1016/j.ceramint.2018.04.258.
[72] G. Podaru, V. Chikan, Chapter 1: Magnetism in nanomaterials: Heat and force from colloidal magnetic particles, Magnetic Nanomaterials: Applications in Catalysis and Life Sciences 2017, pp. 1–24, https://doi.org/10.1039/9781788010375-00001.
[73] G.L. Lima, R.W.L. Oliveira, R.M. de Jesus Neto, De A.M.S. Gomes, R.A. Fiuza Junior, H.M.C. Andrade, A.J.S. Mascarenhas, Single Step Synthesis of Magnetic Materials Derived from Biomass Residues, Waste and Biomass Valorization, 12, 2021 1039–1050, https://doi.org/10.1007/s12649-020-01003-7.
[74] S. Aliramaji, A. Zamanian, Z. Sohrabijam, Characterization and synthesis of magnetite nanoparticles by innovative sonochemical method, Procedia Mater. Sci. 11 (2015) 265–269, https://doi.org/10.1016/j.mspro.2015.11.022.
[75] V.K. Yadav, D. Ali, S.H. Khan, G. Gnanamoorthy, N. Choudhary, K.K. Yadav, V.N. Thai, S.A. Hussain, S. Manhrdas, Synthesis and characterization of amorphous iron oxide nanoparticles by the sonochemical method and their application for the remediation of heavy metals from wastewater, Nanomaterials 10 (2020) 1551–1568, https://doi.org/10.3390/nano10081551.
[76] A. Manikandan, J. Judith Vijaya, L. John Kennedy, M. Bououdina, Structural, optical and magnetic properties of $Zn_{1-x}Cu_xFe_2O_4$ nanoparticles prepared by microwave combustion method, J. Mol. Struct. 1035 (2013) 332–340, https://doi.org/10.1016/j.molstruc.2012.11.007.
[77] H. Fathi, S.M. Masoudpanah, S. Alamolhoda, H. Parnianfar, Effect of fuel type on the microstructure and magnetic properties of solution combusted Fe_3O_4 powders, Ceram. Int. 43 (2017) 7448–7453, https://doi.org/10.1016/j.ceramint.2017.03.017.
[78] M.J. Rivera-Chaverra, E. Restrepo-Parra, C.D. Acosta-Medina, A. Mello, R. Ospina, Synthesis of oxide iron nanoparticles using laser ablation for possible hyperthermia applications, Nanomaterials 10 (2020) 2099–2111, https://doi.org/10.3390/nano10112099.
[79] M. Ajdary, M.A. Moosavi, M. Rahmati, M. Falahati, M. Mahboubi, A. Mandegary, S. Jangjoo, R. Mohammadinejad, R.S. Varma, Health concerns of various nanoparticles: a review of their in vitro and in vivo toxicity, Nanomaterials 8 (2018) 634–662, https://doi.org/10.3390/nano8090634.
[80] S.H. Huang, R.S. Juang, Biochemical and biomedical applications of multifunctional magnetic nanoparticles: a review, J. Nanopart. Res. 13 (2011) 4411–4430, https://doi.org/10.1007/s11051-011-0551-4.
[81] O. Veiseh, J.W. Gunn, M. Zhang, Design and fabrication of magnetic nanoparticles for targeted drug delivery and imaging, Adv. Drug Deliv. Rev. 62 (2010) 284–304, https://doi.org/10.1016/j.addr.2009.11.002.
[82] S.F. Medeiros, J.O.C. Filizzola, V.F.M. Fonseca, P.F.M. Oliveira, T.M. Silva, A. Elaissari, A.M. Santos, Synthesis and characterization of stable aqueous dispersion of functionalized double-coated iron oxide nanoparticles, Mater. Lett. 160 (2015) 522, https://doi.org/10.1016/j.matlet.2015.08.026.
[83] E. Tombacz, R. Turcu, V. Socoliuc, L. Vékás, Magnetic iron oxide nanoparticles: recent trends in design and synthesis of magneto responsive nanosystems, Biochem. Biophys. Res. Commun. 468 (2015) 442–453, https://doi.org/10.1016/j.bbrc.2015.08.030.
[84] P. Tartaj, M. del Puerto Morales, S. Veintemillas-Verdaguer, T. González-Carreño, C.J. Serna, The preparation of magnetic nanoparticles for applications in biomedicine, J. Phys. D. Appl. Phys. 36 (2003) R182–R197, https://doi.org/10.1088/0022-3727/36/13/202.
[85] S. Shukla, A. Jadaun, V. Arora, R.K. Sinha, N. Biyani, V.K. Jain, In vitro toxicity assessment of chitosan oligosaccharide coated iron oxide nanoparticles, Toxicol. Rep. 2 (2015) 27–39, https://doi.org/10.1016/j.toxrep.2014.11.002.
[86] T. Lam, P.K. Avti, P. Pouliot, F. Maafi, J.C. Tardif, É. Rhéaume, F. Lesage, A. Kakkar, Fabricating water dispersible superparamagnetic iron oxide nanoparticles for biomedical applications through ligand exchange and direct conjugation, Nanomaterials 6 (2016) 100, https://doi.org/10.3390/nano6060100.
[87] T.T.D. Tran, T.V. Vo, P.H.L. Tran, Design of iron oxide nanoparticles decorated oleicacid and bovine serum albumin for drug delivery, Chem. Eng. Res. Des. 94 (2015) 112–118, https://doi.org/10.1016/j.cherd.2014.12.016.
[88] T. Muthukumaran, J. Philip, Effect of phosphate and oleic acid capping on structure, magnetic properties and thermal stability of iron oxide nanoparticles, J. Alloys Compd. 689 (2016) 959–968, https://doi.org/10.1016/j.jallcom.2016.08.067.
[89] P. Velusamy, S. Chia-Hung, A. Shritama, G. Venkat Kumar, V. Jeyanthi, K. Pandian, Synthesis of oleic acid coated iron oxide nanoparticles and its role in anti-biofilm activity against clinical isolates of bacterial pathogens, J. Taiwan Inst. Chem. Eng. 59 (2016) 450–456, https://doi.org/10.1016/j.jtice.2015.07.018.
[90] D.R. Ingram, C. Kotsmar, K.Y. Yoon, S. Shao, C. Huh, S.L. Bryant, T.E. Milner, K.P. Johnston, Superparamagnetic nanoclusters coated with oleic acid bilayers for stabilization of emulsions of water and oil at low concentration, J. Colloid Interface Sci. 351 (2010) 225–232, https://doi.org/10.1016/j.jcis.2010.06.048.
[91] Y. Huang, B. Zhang, S. Xie, B. Yang, Q. Xu, J. Tan, Superparamagnetic iron oxide nanoparticles modified with tween 80 pass through the intact blood-brain barrier in rats under magnetic field, ACS Appl. Mater. Interfaces 8 (2016) 11336–11341, https://doi.org/10.1021/acsami.6b02838.
[92] B.J. Palla, D.O. Shah, Stabilization of high ionic strength slurries using surfactant mixtures: molecular factors that de-termine optimal stability, J. Colloid Interface Sci. 256 (2002) 143–152, https://doi.org/10.1006/jcis.2002.8648.
[93] C. Vasilescu, M. Latikka, K.D. Knudsen, V.M. Garamus, V. Socoliuc, R. Turcu, E. Tombácz, D. Susan-Resiga, R.H.A. Ras, L. Vékás, High concentration aqueous magnetic fluids:structure, colloidal stability, magnetic and flow properties, Soft Matter 14 (2018) 6648, https://doi.org/10.1039/C7SM02417G.

Aylin Căpraru is PhD Student at Faculty of Industrial Chemistry and Environmental Engineering. She has MSc studies in Environmental Engineering and Management in Industry and a BSc degree in the same field. Since 2019 until present she is Junior Manager Regulatory Affairs at B. Braun Shared Services, Timişoara, Romania. Her PhD research focus on development and characterization of materials with controlled properties, based on magnetic nanoparticles, with possible applications in cancer therapy and environmental protection. She has knowledge in powder preparation, using the combustion method and also colloids preparation, in order to obtain biocompatible colloidal suspensions.

Elena-Alina Moacă is Lecturer at Department of Toxicology and Drug Industry. She has a PhD. in Chemical Engineering, since 2014 and currently, she is PhD Student at Faculty of Pharmacy. In 2014 she gained a postdoctoral position at the National Institute for Research and Development in the Pathology Domain and Biomedical Sciences "Victor Babes" Bucharest. Technical skills and competences: synthesis of narrow size magnetic iron oxides nanoparticles using co-precipitation/combustion method; synthesis of magnetic composites „core-shell" type; the coating process of nanoparticles with organic/inorganic compounds; production of magnetic nanofluids based on polar/non-polar carriers; production of biocompatible colloidal suspensions for biomedical applications.

Cornelia Păcurariu is Professor at Faculty of Industrial Chemistry and Environmental Engineering; PhD coordinator in the field of Chemical Engineering; Partner in Erasmus Bilateral Agreement with Charles University in Prague. She has teaching and research activities in the field of: Chemical kinetics, Applied physical chemistry, Physical chemistry of interfaces, Nanomaterials synthesis, Environmental protection. She is expert in recipe elaboration/recipe optimization for powder preparation and colloidal suspensions, steric and electrostatic stabilization of powders. She has competences in use and interpretation of thermal analysis (DSC, DTA, TG) and spectroscopic analysis (FT-IR, UV-VIS).

Robert Ianoş is a Professor at Faculty of Industrial Chemistry and Environmental Engineering within Politehnica University of Timisoara (WOS ResearcherID: B-7271-2011). He has an Habilitation certificate in the field of Chemical Engineering. His didactic activity is focused on nanomaterials, composite materials, solid state physical chemistry, physical chemistry of interfaces and colloidal chemistry. The main research field of Robert IANOŞ is the preparation of metal oxide (nano)particles via solution combustion synthesis, with a special emphasis on NIR-reflective pigments, ceramic pigments and iron oxide nanoparticles for biomedical applications.

Radu Lazău is Associate Professor at Faculty of Industrial Chemistry and Environmental Engineering with a PhD diploma in Materials Science and Engineering. He is an experienced researcher in the field of synthesis and characterization of oxide materials with various applications, including pigments, glazes, cool coatings and phosphor materials. Experienced user trained in using the following research equipment/interpretation of the results: Rigaku ULTIMA IV X-ray diffractometer; Micromeritics ASAP 2020 Specific surface measurement instrument; VARIAN Cary 300 Bio spectrophotometer. 57 research papers in ISI journals, Hirsch index h = 13, main author/co-author of 4 books, 1 book chapter in an international publishing house.

Lucian Barbu-Tudoran is Associate Professor at Faculty of Biology and Geology, PhD in Biology. Since 2009 he is Manager of the Electron Microscopy Centre. Expert in physical-chemical and morphological characterization of nanomaterials used as vectors for therapy, for new technologies, or for bio-detection; ultrastructural characterization of tumor lines and the effects of various drugs on them; biological samples preparation. He has worked as a postdoctoral fellow in a Marie Curie scholarship (University of Leeds, UK) and he has specialized courses: Cryo-Electron Microscopy in Life Science; Cryo-Electron Microscopy of Vitreous Sections; Combination of Electron Microscopy and X-Ray Crystallography for structure determination.